International Journal of Geosynthetics and Ground Engineering (2025) 11:69
https://doi.org/10.1007/s40891-025-00675-2

ORIGINAL PAPER

Integrating Supervised Machine Learning with Laboratory Data To Evaluate the Modulus Improvement Factor in Geocell-Reinforced Soils

H. D. Trujillo[1] · **J. O. Avesani Neto**[1] · **J. G. Zornberg**[2]

Received: 29 May 2025 / Accepted: 2 November 2025

Abstract
This article presents the analysis of results from Plate Load Tests (PLT) involving a series of load-unload-reload cycles. A total of 128 tests were conducted to investigate the parameters governing the Modulus Improvement Factor (MIF) based on the performance of unreinforced and geocell-reinforced coarse materials under varied conditions. A soft clay and a sandy soil, prepared at three different relative densities, were used as subgrade. The geocell infill material consisted of sandy soil and Granular Subbase (GSB) material, placed at two different densities each. Two types of HDPE geocells with different dimensions were used. Multilayer Perceptron (MLP) neural networks were used to analyze the combined influence of the various parameters on MIF. The results show that MIF has an increasing trend with increasing subgrade modulus, and a decreasing trend with increasing geocell pocket size and infill material modulus. Overall, the MLP was identified as a suitable tool for parametric analyses to assess the benefits of geosynthetics in roadway applications.

Keywords Geosynthetics · Subgrade · Infill material · Neural networks · Deep learning

List of symbols

D_r	Relative density (%)
e_{max}	Maximum void ratio (dimensionless)
e_{min}	Minimum void ratio (dimensionless)
E_R	Modulus of the reinforced infill layer (MPa)
E_s	Modulus of subgrade (MPa)
E_{s_R}	Modulus of the subgrade supporting the reinforced infill material layer (MPa)
E_{s_un}	Modulus of the subgrade supporting the unreinforced infill material layer (MPa)
E_{surf}	Surface modulus (MPa)
E_{surf_R} (MPa)	Surface modulus with reinforcement (MPa)
E_{surf_un} (MPa)	Surface modulus in the absence of reinforcement (MPa)
E_{un} (MPa)	Modulus of unreinforced infill layer (MPa)
k	Modulus number (dimensionless)
RC	Relative compaction
R^2	Coefficient of determination
S_i	Relative stiffness of the reinforcement
S_u	Undrained shear strength (kPa)
w_n	Natural water content (%)
w_{opt}	optimum water content (%)
γ_d	Dry unit weight (kN/m^3)
γ_s	Unit weight of solids (kN/m^3)

✉ H. D. Trujillo
hectortrujillo@usp.br

J. O. Avesani Neto
avesani@usp.br

J. G. Zornberg
zornberg@mail.utexas.edu

[1] Department of Structural and Geotechnical Engineering, Escola Politécnica at Universidade de São Paulo (EP-USP), Av. Professor Almeida Prado, travessa 2 nº 83, São Paulo 05508-010, SP, Brazil

[2] Department of Civil, Architectural and Environmental Engineering, The University of Texas at Austin, 301 E. Dean Keeton St, Austin, Texas 78712, USA

Introduction

Geocells can be used in the design of many geotechnical projects, including embankments, foundations, slope stabilization, erosion control, retaining walls, protection of

Published online: 25 November 2025

buried pipelines, and paved and unpaved roads [1–8]. In Transportation Infrastructure projects, their typical function involves the stiffening of the unbound granular layers of roadway structures [9, 10].

In pavement design using the Mechanistic-Empirical Pavement Design Guide (MEPDG), the elastic parameters are particularly significant parameters to characterize the unbound aggregate layers [11, 12]. The increase in modulus in a layer reinforced with geocells can be captured by the Modulus Improvement Factor (MIF), defined as the ratio between the modulus in the reinforced condition to that in the unreinforced condition [13, 14]. Typically reported magnitudes of MIF have ranged from 1.5 to 5.0 based on laboratory experiments, although the reported magnitudes have ranged from 2.0 to 4.0 when the parameters are back-calculated from in-service roadway applications or full-scale tests [9, 14–18]. The characteristics of the infill soil, the geocell, the infill compaction process, and the subgrade layer can influence the MIF [19, 20]. Due to the complexity involved in quantifying the MIF, some studies have recommended using analytical methods or conducting specific laboratory tests to predict it for the specific conditions of roadway projects [9, 21].

The Plate Load Test (PLT) is probably the most common laboratory test used to quantify the improvement resulting from the inclusion of geocells. Specifically, the performance of geocell-reinforced soil has been studied extensively through PLT to assess the influence of parameters such as the infill material properties, subgrade conditions, and geocell characteristics [22–24]. However, the study of these factors has mainly focused on the Ultimate Limit State (ULS) and not on the Serviceability Limit State (SLS), which is the basis of the MEPDG [19].

Recent studies using Artificial Intelligence (AI) — specifically neural networks — have shown promising results in predicting the settlement and vertical stresses in geocell-reinforced soils subjected to PLT [25–28]. Although the application of neural networks in geocell performance analysis is still emerging, these studies suggest that this approach can reliably enhance the prediction process, as it considers the complex interactions among various influencing factors.

In this context, the main objective of this paper is to evaluate the influence of infill material, subgrade conditions, and geocell geometry on MIF values. As part of the experimental program, numerous PLTs were conducted to subsequently back-calculate the moduli of unreinforced and reinforced layers under different conditions. The obtained MIF values were then analyzed using neural network models. These models were employed to predict and interpret the results, as well as to generate charts correlating the relevant variables.

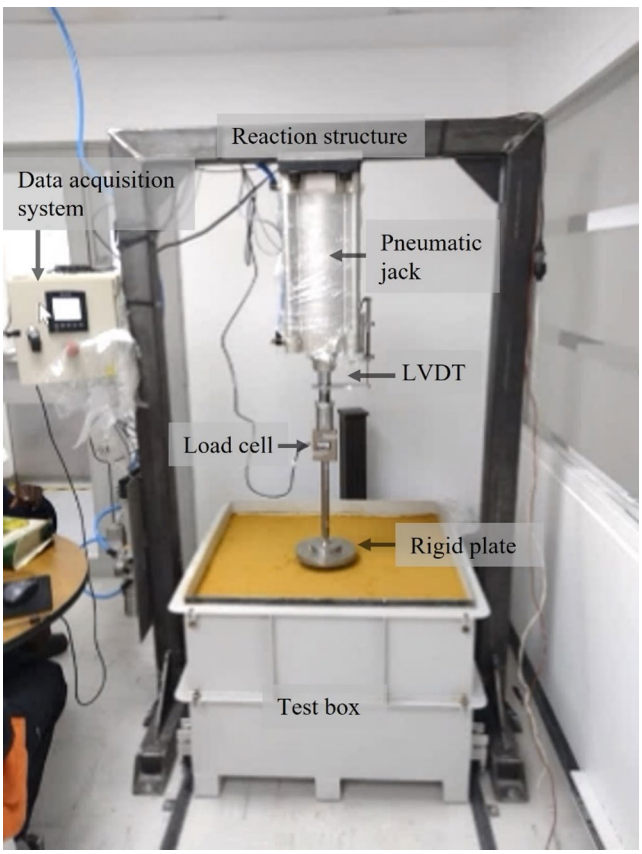

Fig. 1 PLT laboratory test setup

Laboratory Model Tests

Testing Setup and Procedures

The laboratory model, presented in Fig. 1, consisted of a metallic test box in which both reinforced and unreinforced soil layers were constructed and subsequently subjected to PLT. The box measured 0.8 m x 0.8 m x 0.9 m (length x width x height) and was rigid enough to minimize lateral displacements. A computer-controlled pneumatic actuator was used to apply pressure to a circular metal plate with a diameter of 200 mm. A load cell and a Linear Variable Differential Transformer (LVDT), connected to a data acquisition system, were used to record the load and settlement during testing. In these tests, which followed the German standard DIN 18134 [29], the first loading cycle was considered complete when either a maximum load of 600 kPa or a maximum settlement of 8 mm was reached, whichever occurred first. After which unloading and subsequent reloading followed. The maximum load for the reload cycle was the same as that reached in the first cycle.

The experimental study was conducted in four series, each with 16 laboratory model tests, involving a two-layer

Table 1 Configurations of the two-layer models in this study

Series	Configuration	Subgrade	Top layer	Thickness of top layer (cm)	Reinforcement	Layers tested per config.
1	1	Sand (Dr = 20%)	Sand (Dr = 50%)	13	Unreinforced	Subgrade and Top layer
	2			16	Unreinforced	
	3			13	Geocell A	
	4			16	Geocell B	
	5		Sand (Dr = 80%)	13	Same as configurations 1 to 4	
	6			16		
	7			13		
	8			16		
	9		GSB (RC = 95%)	13	Same as configurations 1 to 4	
	10			16		
	11			13		
	12			16		
	13		GSB (RC = 100%)	13	Same as configurations 1 to 4	
	14			16		
	15			13		
	16			16		
2	17 to 32	Sand (Dr = 50%)	Same as Series 1			
3	33 to 48	Sand (Dr = 80%)				
4	49 to 64	Soft clay				
Total PLTs						128

Table 2 Properties of the different soils in this study

Material	Sand	GSB	Soft clay
Unit weight of solids, γ_s (kN/m^3)	24.0	25.6	24.3
Fines content (%)	11.9	16	90
Liquid Limit, LL	-	21	48
Plastic Limit, PL	-	11	26
Plasticity Index, PI	-	10	22
USCS classification	SP-SM	GC	CL
HRB classification	A-2–4	A-2–4	A-7-6 (18)
Undrained shear strength, S_u (kPa)	-	-	9
Friction angle, φ' (°)	28.4	38.5	-
California Bearing Ratio, CBR (%)	-	18.5	1.2

system configuration (i.e., a subgrade layer and a granular unreinforced or geocell-reinforced top layer), as summarized in Table 1. Each configuration involved two tests (one per layer), resulting in a total of 128 PLT conducted in this study. The subgrade in Series 1, 2, and 3 consisted of a sand layer placed at relative densities (D_r) of 20%, 50%, and 80%, respectively. A soft clay layer was used as subgrade in Series 4. The top layer in all four series consisted of a sand layer placed at D_r of 50% and 80%, as well as a material identified as Granular Subbase (GSB) placed at a relative compaction (RC) of 95% and 100% in relation to the maximum dry unit weight obtained from Modified Proctor Compaction tests. Two geocells (Geocells A and B) with distinct geometries were used for the reinforced condition. Further details regarding the testing setup and procedures can be consulted in Trujillo [30].

Materials

The sand used in this study was obtained from a quarry located in the southern region of Bogotá, Colombia, and served both as subgrade, with D_r of 20%, 50%, and 80% in Series 1, 2, and 3, respectively, and as infill material with D_r of 50% and 80% in all series (Table 1).

The sand had a fines content of 11.9% (fraction of particles smaller than 75 µm), a unit weight of solids (γ_s) equal to 24 kN/m^3, no plasticity, and was used in dry condition during the tests. The minimum void ratio (e_{min}) and maximum void ratio (e_{max}) were 0.31 and 0.79, respectively, with corresponding maximum and minimum dry unit weights of 18.3 and 13.4 kN/m^3. The sand is classified as poorly graded sand with silt (SP-SM) according to the Unified Soil Classification System (USCS) and as A-2–4 according to the Highway Research Board (HRB) system classification. The friction angle (φ') of the sand at 90% D_r was determined as 28.4°, which falls within the typical range reported in the literature for similar soils [31, 32]. Table 2 summarizes the properties of the soil used in this study.

The GSB, used only in the top layer, had a maximum grain size of 38 mm, a fines content of 16%, and γ_s of 25.6 kN/m^3. The liquid limit and plasticity index of the fines fraction were 21 and 10, respectively. The maximum dry unit weight for the Modified Proctor Compaction test was 20.3 kN/m^3 for an optimum water content (w_{opt}) of 7.9%. The φ' of the GSB and California Bearing Ratio (CBR) for Modified Proctor Compaction condition were 38.5° and 18.5%,

respectively. The GSB is classified as a clayey gravel (GC) and a A-2–4 according to the USCS and HRB, respectively.

The soft clay subgrade used in Series 4 consisted of a typical clay from Bogotá, with a fines content of 90%, liquid limit and plasticity index of 48 and 22, respectively. This material is classified as lean clay (CL) and A-7-6 (18) according to the USCS and HRB, respectively. The CBR for the soft clay was determined to be 1.2%. The undrained shear strength (S_u) under undisturbed conditions was 9 kPa. In Series 4, this S_u was achieved by setting the water content at 19%, previously calibrated using a mini vane shear device.

Two types of geocells, manufactured using High-Density Polyethylene (HDPE) were used in this study. Geocell A was characterized by a height of 120 mm, weld spacing of 356 mm for a folded cell, and pocket cell area of 29×10^{-3} m² corresponding to an equivalent diameter (d_{eq}) of 193 mm. Geocell B had a height, weld spacing, pocket cell area, and equivalent diameter of 150 mm, 445 mm, 48×10^{-3} m², and 247 mm, respectively. The walls of both geocells were textured, with 10-mm-diameter perforations covering an area of 10% of the wall area, an elastic modulus equal to 700 MPa, and a thickness of 1.5 mm. Geocells A and B were used to reinforce the top layers with total thicknesses of 130 mm and 160 mm, respectively. A summary of the geocell characteristics is listed in Table 3. Additional information on the material characterization and geocell configuration can be found in Trujillo [30].

Model Preparation

The internal surface of the box was coated with petroleum jelly to minimize sidewall friction effects. The models prepared for Series 1–3 involved initial placement and densification of the sandy subgrade. The test bed was prepared by placing the sandy soil in the box and compacting it in 100-mm-thick sublayers until reaching the target height. For each densified sublayer, the amount of soil required to achieve the target D_r was weighed and placed in the test box. Compaction was performed using the tamping method, employing a manual compactor consisting of a lightweight steel bar with a flat square base. The compaction energy was adjusted empirically through preliminary trials to achieve the target dry densities. For the case of the 20% D_r, the sand was gently tamped to preserve the loose state, consistent with previous reports in the literature [33]. It is important to note that, after reaching the target D_r, the density of the subgrade was verified before the construction of the upper layer. Since a small manual compactor with limited compactive energy was employed, the stresses transmitted during placement of the top layer were substantially lower than those applied in field operations [17, 18], thereby minimizing the risk of further densification of the underlying subgrade. This procedure ensured that the intended relative densities of 20%, 50%, and 80% were preserved within acceptable tolerance.

Table 3 Summary of geocell characteristics [57]

Properties	Geocell A	Geocell B
Polymer	HDPE	HDPE
Weld spacing (mm)	356	445
Density (g/cm³)	0.945–0.960	0.945–0.960
Open cell dimensions (mm)	259 × 226	315 × 304
Cell wall height (mm)	120	150
Pocket cell area (m²)	29×10^{-3}	48×10^{-3}
Equivalent diameter (mm)	193	247
Cell wall thickness (mm)	1.5	1.5
Elastic modulus (MPa)	700	700

In Series 4, the clayey soil was first pulverized and then mixed with water to reach a water content of 19%. Additionally, to verify uniformity after placement and compaction, the S_u was measured using a mini vane shear device. Test bed preparation followed the same procedure as that for Series 1–3. The first PLT were carried out after completing the placement of the subgrade. Given the high water content of this clay, particular care was taken during construction of the overlying granular layers. The sand used as infill was placed in dry condition, and the relatively short time between placement and testing minimized the possibility of water migration. Therefore, no thick moist-sand interface was observed to develop, and the clay–sand boundary maintained the properties of each constituent layer throughout the duration of the experiments.

A procedure similar to that followed for the placement of the sandy soil was carried out for preparation of the top soil layer. For the GSB, after the w_{opt} was reached, the mixture was homogenized and compacted with previously adjusted energy to achieve a target γ_d corresponding to a RC of 95 and 100%, respectively, according to the Modified Proctor. Density control for the GSB consisted of checking the required weight of water and material for its total thickness. Again, the use of manual compaction resulted in lower applied stresses than those of heavy field equipment [17, 18], thus reducing the potential effect on the condition of the underlying subgrade. It is important to note that differences in compaction stress can significantly influence the MIF, which is also influenced by the stresses induced during the process [19].

For the reinforced conditions, the geocells were placed and fixed to the sides of the test box using steel bars driven into the subgrade, ensuring contact between the center of the circular plate and the junctions of four open cells. The granular material was then deposited and compacted, after which a second PLT was performed to generate the stress-displacement curve of the two-layer system. Further

information on the model preparation is provided in Trujillo [30].

Results and Discussion

Plate load tests (PLTs) were carried out directly over the subgrade and top layer in each configuration to obtain stress-displacement curves. The moduli of the subgrade material (E_s) were obtained from the first set of PLT tests conducted after subgrade construction. Also, the equivalent moduli of the two-layer system (i.e. subgrade + top layer, E_{surf}) were obtained from the second set of PLT tests conducted after the construction of the top layer [13, 17, 34]. The moduli were determined using an extension of the Boussinesq equation for a homogeneous and isotropic semi-infinite mass subjected to a rigid circular load, as follows:

$$E = \frac{\sigma}{s} B(1 - v^2) C_s \quad (1)$$

where E is the elastic modulus; σ is the applied stress corresponding to a deflection s; B is the plate diameter (200 mm); ν is the Poisson's ratio; and C_s is a geometric factor (0.79 for the center of a rigid circular load).

A Poisson's ratio was adopted for each layer based on values typically reported in the literature for similar soils and conditions [7, 12, 17, 18, 35–37]. The sandy soil with 20% D_r was assigned a Poisson's ratio of 0.30; both sandy soil with 50% and 80% D_r and the GSB layer were assigned a value of 0.35; the soft clay was assigned a value of 0.45; and the geocell-reinforced layers were assigned a value of 0.25. Although adopting representative values for Poisson's ratio may be a simplification, its effect on determining the MIF is expected to be marginal, since the MIF is calculated based on the relationship between reinforced and unreinforced modulus.

Moduli (E_s and E_{surf}) were obtained by back analysis of the PLT results. Specifically, the stress-displacement pair on the reload-unload cycle was analyzed following the German standard DIN 18,134 [29]. To single out the top layer modulus using both E_s and E_{surf} (the latter obtained from the PLT conducted over the top layer), the analytical equation by Avesani Neto [34], based on two-layered elastic system solutions, was employed following the methodology of Zipoli and Avesani Neto [17] and Feng et al. [18].

The following sections initially present the PLT results, followed by the analysis of the corresponding moduli and MIF, as well as the evaluation of the influence of the subgrade, infill material and geocell geometry. Finally, design charts are provided to correlate the relevant variables affecting the MIF using multilayer perceptron models.

Layer Moduli and MIF Results

Table 4 summarizes the results obtained for each configuration described in Table 1. The first column presents the test series (1 to 4). The second column indicates the pair of unreinforced (un) and reinforced (R) models with the same soil layer configuration. The third and fourth columns detail the materials for the top layer. The fifth and sixth columns present the subgrade moduli for the unreinforced (E_{s_un}) and reinforced (E_{s_R}) conditions of the top layer, respectively. The seventh and eighth columns show the surface moduli, obtained from PLTs conducted over the top layer, for the unreinforced (E_{surf_un}) and reinforced (E_{surf_R}) conditions, respectively. The ninth and tenth columns show the top layer moduli for the unreinforced (E_{un}) and reinforced (E_R) configurations, respectively. Finally, the eleventh column presents the MIF calculated as the ratio of reinforced to unreinforced top layer modulus (E_R/E_{un}).

Inspection of the results presented in Table 4 confirms the beneficial effect of geocell reinforcement on the top layer modulus in all performed experiments. Specifically, the MIF always exceeded 1.0 for all test configurations, with values ranging from 1.05 to 2.14, with an average of 1.44. As previously mentioned in the Model Preparation section, low compaction stresses were applied to densify the materials. However, even in the absence of relevant compaction, which generates high horizontal stresses inside the cell pocket and is one of the most important factors for increased confinement and MIF [19], a significant improvement was observed in the top layer modulus in reinforced conditions. As previously stated, MIF values are not constant but depend on factors such as subgrade conditions, infill material, and geocell geometry [9, 20, 21, 38].

A review of the sandy soil subgrade moduli in Table 4 reveals that the average value of E_s increases, and the Coefficient of Variation (COV) decreases, with increasing D_r. Specifically, for a 20% D_r (Series 1), the average E_s is 23.5 MPa (with a COV of 22%). As the D_r of the sand increased to 50% (Series 2), E_s rose to 29.0 MPa (with a decreased COV of 17%). Further increase in D_r to 80% (Series 3) resulted in an increased average E_s of 34.8 MPa (with a COV of 18%). These results align with correlations reported in literature between D_r and stiffness of sands [31]. Consistent with this trend, the soft clay subgrade (Series 4) displayed a lower average E_s of 9.4 MPa (with a higher COV of 38%). The E_s values obtained in the laboratory fall within the typical range reported in the literature for different materials [35, 39] as well as within the usual range of variability expected for both sandy soil and soft clays in pavement subgrade [40].

Since the main objective of this study is to evaluate the improvement provided by the geocell inclusion in top layer, the surface moduli are treated as intermediate values used

Table 4 Summary of moduli and MIF obtained in the experimental program

Series/ subgrade	Conf. $_{(Un-R)}$	Top layer/geocell infill material		E_{s_un} (MPa)	E_{s_R} (MPa)	E_{surf_un} (MPa)	E_{surf_R} (MPa)	E_{un} (MPa)	E_R (MPa)	MIF
		Material	Thickness (mm)							
Series 1 Sand D_r = 20%	1–3	Sand − 50%	130	25.7	18.3	25.6	26.6	24.0	41.2	1.72
	5–7	Sand − 80%		16.0	18.4	28.0	32.0	49.9	62.5	1.25
	9–11	GSB − 95%		16.3	16.5	27.7	31.5	47.1	69.7	1.48
	13–15	GSB − 100%		23.7	28.8	49.6	59.3	114.5	147.0	1.28
	2–4	Sand − 50%	160	25.3	20.3	24.7	24.1	22.9	28.6	1.25
	6–8	Sand − 80%		26.2	24.0	36.0	34.2	43.1	46.8	1.08
	10–12	GSB − 95%		27.3	32.6	31.6	39.8	33.0	48.2	1.46
	14–16	GSB − 100%		26.7	29.6	45.9	48.6	67.7	75.6	1.12
Series 2 Sand D_r = 50%	17–19	Sand − 50%	130	27.8	30.0	30.8	40.3	33.9	61.6	1.82
	21–23	Sand − 80%		20.9	24.7	39.3	45.3	85.0	104.1	1.22
	25–27	GSB − 95%		39.3	31.7	51.3	55.2	68.0	117.9	1.74
	29–31	GSB − 100%		30.9	29.5	47.0	52.0	73.7	112.7	1.53
	18–20	Sand − 50%	160	25.3	29.4	28.6	34.4	31.1	43.0	1.38
	22–24	Sand − 80%		23.4	28.7	30.5	36.3	37.3	48.1	1.29
	26–28	GSB − 95%		24.4	37.8	33.0	52.0	41.7	74.0	1.78
	30–32	GSB − 100%		31.4	28.7	44.5	48.7	58.6	84.6	1.44
Series 3 Sand D_r = 80%	33–35	Sand − 50%	130	36.5	38.1	36.5	47.4	36.5	66.5	1.82
	37–39	Sand − 80%		26.9	30.2	44.5	51.4	79.8	106.5	1.33
	41–43	GSB − 95%		43.1	29.6	58.6	57.7	81.3	145.4	1.79
	45–47	GSB − 100%		37.2	27.5	58.2	63.3	96.6	207.0	2.14
	34–36	Sand − 50%	160	38.1	36.4	41.0	48.6	43.2	67.5	1.56
	38–40	Sand − 80%		28.1	44.0	42.2	54.6	58.7	71.4	1.22
	42–44	GSB − 95%		35.1	38.1	48.3	67.1	61.9	120.7	1.95
	46–48	GSB − 100%		43.4	24.8	57.0	52.6	70.1	116.3	1.66
Series 4 Soft clay	49–51	Sand − 50%	130	11.3	4.6	14.3	8.4	22.2	23.9	1.08
	53–55	Sand − 80%		10.6	9.3	17.7	16.1	40.5	42.7	1.05
	57–59	GSB − 95%		11.6	11.9	15.4	17.2	25.5	35.5	1.39
	61–63	GSB − 100%		7.9	9.5	12.9	14.4	25.6	31.0	1.21
	50–52	Sand − 50%	160	6.1	5.0	8.5	8.3	13.3	17.1	1.28
	54–56	Sand − 80%		15.5	10.1	17.6	13.9	22.8	23.9	1.05
	58–60	GSB − 95%		5.3	4.3	11.2	10.6	27.9	35.5	1.27
	62–64	GSB − 100%		14.7	12.9	20.4	20.6	31.6	40.6	1.28

solely for back-calculating the moduli of the top layer. Therefore, they are not analyzed herein.

The results in Table 4 show that the use of geocells led to an increase in the moduli of the top layer, generating the observed MIF values (E_R/E_{un}). These results also indicate that the subgrade material and condition, infill material and geocell geometry influence the MIF value. A detailed analysis of these parameters is presented in the following sections.

Influence of the Infill Material

Figures 2 and 3 present the influence of the infill material on the top layer moduli and MIF for the two geocells investigated in this study. Specifically, Fig. 2a and c show the top layer moduli of the sandy soil infill at D_r of 50% and 80% for unreinforced and geocell-reinforced cases (Geocell A and B, respectively), while Fig. 2b and d show the corresponding MIF values. Figure 3a and c show the top layer moduli of the GSB infill at RC of 95% and 100% for unreinforced and Geocell-reinforced cases (Geocells A and B, respectively), and Fig. 3b and d show the corresponding MIF values.

The results in Figs. 2 and 3 indicate that the material type in the top layer, as well as its density, significantly influences the top layer moduli in relation to that in the unreinforced condition. Overall, the GSB exhibited a higher unreinforced modulus—an average of 44% higher—than the sandy soil. Increased densification of the top layer material also promoted higher modulus independent of the material type. Specifically, an increase in the sandy soil D_r from 50% to 80% caused an increase in its modulus from 20% to 151% (84% on average). Similarly, increasing the RC of the GSB

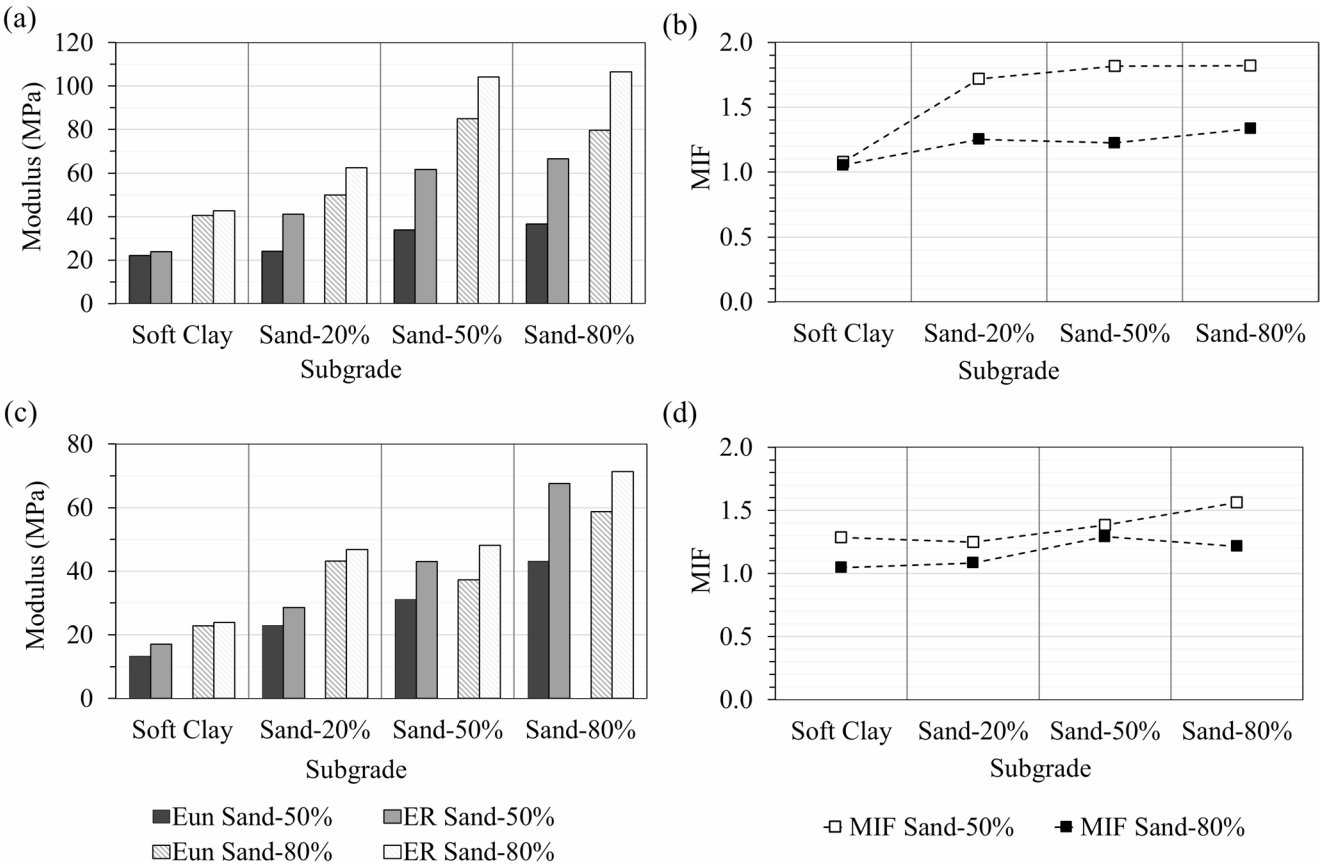

Fig. 2 Influence of subgrade and D_r of sandy soil infill on moduli and MIF: **a** unreinforced and Geocell A-reinforced modulus; **b** MIF for Geocell A; **c** unreinforced and Geocell B-reinforced modulus; and **d** MIF for Geocell B

from 95% to 100% led to an increase in the GSB modulus from 0.3% to 143% (average of 39%).

The results in Figs. 2 and 3 also show the impact of the different variables on the MIF. Specifically, MIF values ranging from 1 to 1.8 (averaging 1.3) were obtained for the cases involving sandy soil infill, while such values ranged from 1.1 to 2.1 (averaging 1.5) for the cases involving GSB infill. Although E_{un} and E_R were consistently higher in conditions involving infill with higher density, the MIF did not show a proportional increase. In fact, as observed in Figs. 2 and 3, the MIF was consistently higher for the less dense condition (dashed lines). This behavior can be attributed to the comparatively low compaction energy used to densify the materials and to the soil-geocell interaction. This interaction is quantified by the soil-reinforcement relative stiffness index (S_i), which is expected to have a significant influence on the MIF values [19]. The S_i (Eq. 2) is defined as the ratio of the geocell wall stiffness (J) to the product of the atmospheric pressure (P_a), the equivalent cell diameter (d_{eq}) and the soil modulus number (k) in the hyperbolic constitutive model [41].

$$S_i = \frac{2J}{kP_a d_{eq}} \tag{2}$$

The stiffness of the infill soil is represented by the modulus number (k) in Eq. 2. Soils with lower density (higher porosity) exhibit lower stiffness, i.e., a reduced modulus number [42, 43]. Thus, small k values correspond to a higher S_i, significantly increasing the MIF [19].

Therefore, since very low compaction energy was used in the soil densification process for all experimental configurations, the less dense soils (more porosity) had smaller k values, which can be attributed to lead to comparatively higher MIF results, as reported in literature [9, 19, 20].

Influence of the Subgrade

The results in Figs. 2 and 3 are also useful to assess the influence of the subgrade material and its condition on the moduli of the top layer and MIF values for both geocells. It can be observed that both unreinforced and reinforced moduli significantly increase with increasing subgrade modulus. The soft clay subgrade was the least stiff material (average E_s of 9.4 MPa in Table 4) and resulted in comparatively

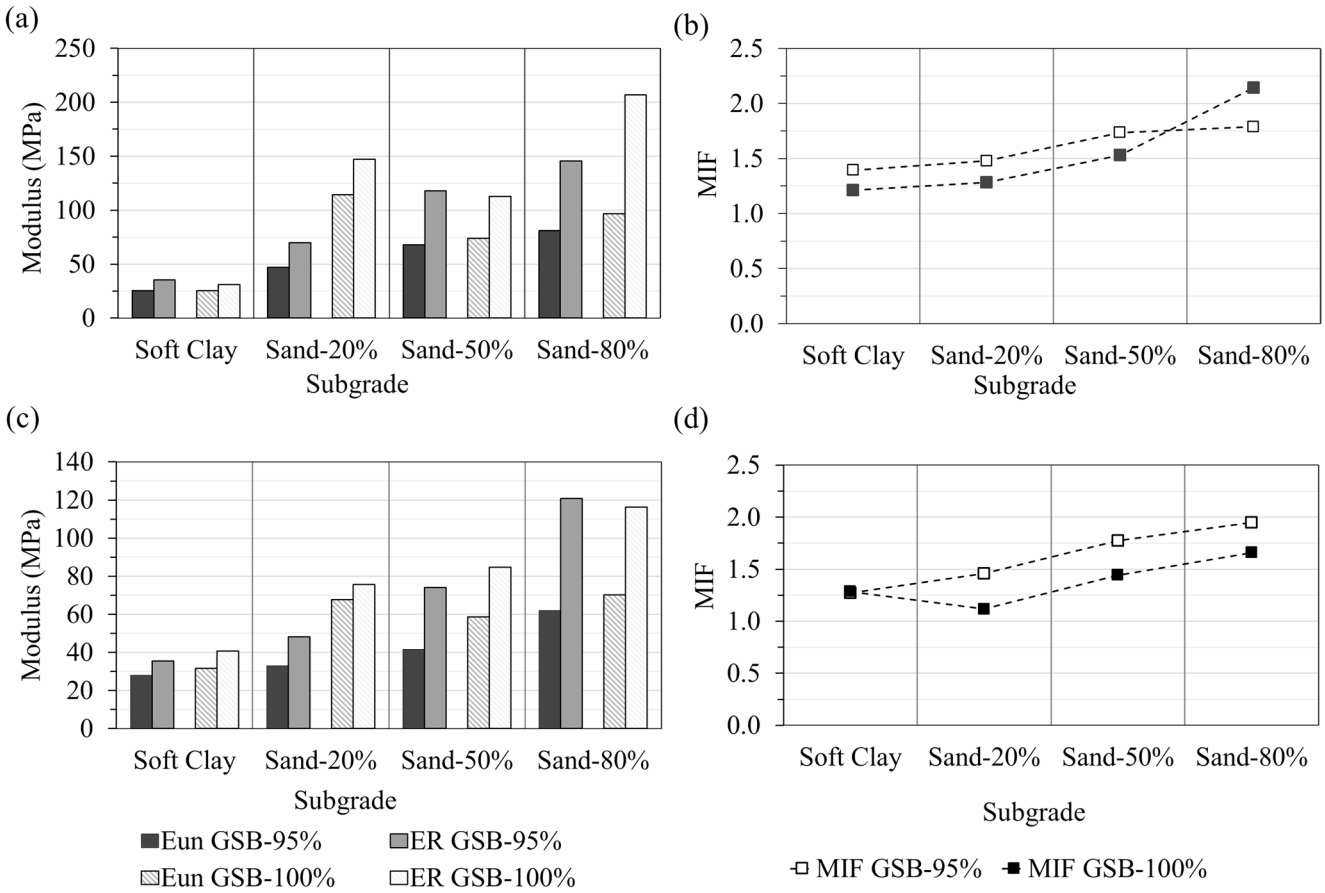

Fig. 3 Influence of subgrade and RC of GSB infill on moduli and MIF: **a** unreinforced and Geocell A-reinforced modulus; **b** MIF for Geocell A; **c** unreinforced and Geocell B-reinforced modulus; and **d** MIF for Geocell B

smaller moduli for the two top layer materials evaluated in this study. Specifically, the average moduli are 25 MPa and 27 MPa for the unreinforced and reinforced conditions, respectively, for the cases involving sandy soil infill. The average moduli are 28 MPa and 36 MPa for the unreinforced and reinforced conditions, respectively, for the cases involving GSB infill. The sandy soil subgrade with a D_r of 20% was stiffer than the soft clay (average E_s of 23.5 MPa in Table 4), resulting in an increase in the top layer unreinforced moduli for the sandy soil and GSB, averaging 42% and 137%, respectively, in relation to those obtained with soft clay. The same sandy soil subgrade, but with a higher D_r of 50% (average E_s of 29.0 MPa in Table 4) resulted in an increased unreinforced modulus of the top layer by an average of 90% and 119% for the sandy soil and GSB infills, respectively, compared to the soft clay subgrade. The sandy soil subgrade with a D_r of 80% (average E_s of 34.8 MPa in Table 4) resulted in a further increase of the unreinforced moduli, corresponding to an average of 121% and 180% for the sandy soil and GSB, respectively, again compared to the soft clay subgrade. Comparing the results for only the sandy soil subgrade, the increase in D_r from 20% to 50% resulted in an increase in the top layer unreinforced moduli for the sandy soil of 34% in average. Similarly, the increase in D_r from 50% to 80% resulted in an average improvement of 16% and 28%, respectively, for the sandy soil and GSB. The relationship between the average E_{un} and E_s was determined from the data, which exhibited a linear trend and indicated proportionality between these two variables, with increasing rates (i.e. the slope of the relationship) of 1.8 and 1.2 for the GSB and sandy soil infills, respectively.

The influence of the bottom layer stiffness on the modulus of the unbound granular material's upper layer has been investigated in previous studies, resulting in trends similar to those observed herein [9, 12, 17, 44, 45]. This trend can be attributed to a lack of support from the bottom layer. That is, since the unbound granular materials of the upper layer are sensitive to confinement, a lack of support from the bottom layer, especially during the compaction process, results in a reduced upper layer confinement, ultimately leading to a decrease in its modulus.

In fact, some authors have introduced a factor that represents the maximum increase in stiffness of unreinforced, unbound granular material relative to the stiffness of the

underlying layer [9, 44]. This limitation on the maximum stiffness of materials sensitive to confinement is also indicated in several pavement design manuals, which state that the stiffness of an unbound granular layer depends not only on the thickness of the layer but also on the stiffness of the underlying material [12, 46, 47].

Figures 2 and 3 also reveal that the MIF was affected by the subgrade condition following trends consistent with those in previous studies [9]. This behavior can again be explained by the low compaction stresses used to densify the geocell infill materials. Since the compaction process did not generate significant stresses in the top layer, the stiffness of the subgrade had a significant influence on the MIF. When comparatively high stresses are induced by the compaction process, higher residual stresses are induced within the infill material, as lateral deformation is restricted by the geocell walls [48]. Consequently, the geocell reinforcement can compensate for the subgrade-induced lack of confinement, improve the upper layer modulus more efficiently, ultimately minimizing the subgrade influence on the MIF value [9, 17, 18].

The average MIF obtained for the upper layer resting on the soft clay subgrade, as depicted in Figs. 2 and 3, ranged from 1.0 to 1.4 (an average of 1.2). The average MIF increased by approximately 11%, from the soft clay subgrade to the sandy soil subgrade with a D_r of 20%, reaching a value of 1.3. The average MIF also reached a value of 1.5 (about 27% higher than for the soft clay subgrade) and 1.7 (approximately 40% higher than for the soft clay subgrade) for the sandy soil subgrade with a D_r of 50% and 80%, respectively. Comparing only the cases involving sandy soil subgrade, the increase in subgrade D_r from 20% to 50% and from 20% to 80% increased the average MIF by 15% and 27%, respectively. Additionally, the D_r increase from 50% to 80% improved the MIF by an average of 10%.

Influence of the Geocell Dimensions

Figure 4 shows the average MIF obtained in all experiments with Geocell A and Geocell B, for both the sandy soil and GSB as infill materials with different subgrade materials and conditions.

The results in Fig. 4 indicate that Geocell A generally showed greater improvement than Geocell B, except in the case of the sand infill with the soft clay subgrade. For the cases involving GSB infill, in the different subgrade conditions, Geocell A exhibited a higher MIF than Geocell B, with values between 1% and 9% higher (5% higher on average), compared to Geocell B. For the cases involving sandy soil infill, Geocell A presented a maximum MIF increase of 27%, compared to Geocell B in the sandy subgrade with 20% D_r, and an average of 12% for all subgrade conditions. When all experiments are considered, Geocell A generated a MIF value 8% higher than Geocell B. The geometry of Geocell A is characterized by a d_{eq} of 193 mm and height of 120 mm; while Geocell B dimensions involved a d_{eq} of 247 mm and a height of 150 mm. The trends observed in Fig. 4 seems to be governed by the d_{eq} of the geocells. As shown by Garcia and Avesani Neto [19], the d_{eq} is an important parameter for the S_i (Eq. 2): an increase in d_{eq} leads to a reduction in the S_i and, consequently, the MIF. Although the geocell height influences the surface modulus obtained from PLTs, the layer modulus is only marginally affected by the geocell height.

Combined Effect of subgrade, infill, and Geocell Dimensions

The analyses of the 128 PLT presented in the previous subsections confirm that the infill, subgrade, and geocell dimensions influence MIF values. Despite the large number of PLTs conducted in this study, many additional variable combinations remain untested, as a parametric investigation accounting for the multiple remaining combinations would be prohibitive. Consequently, a parametric evaluation to

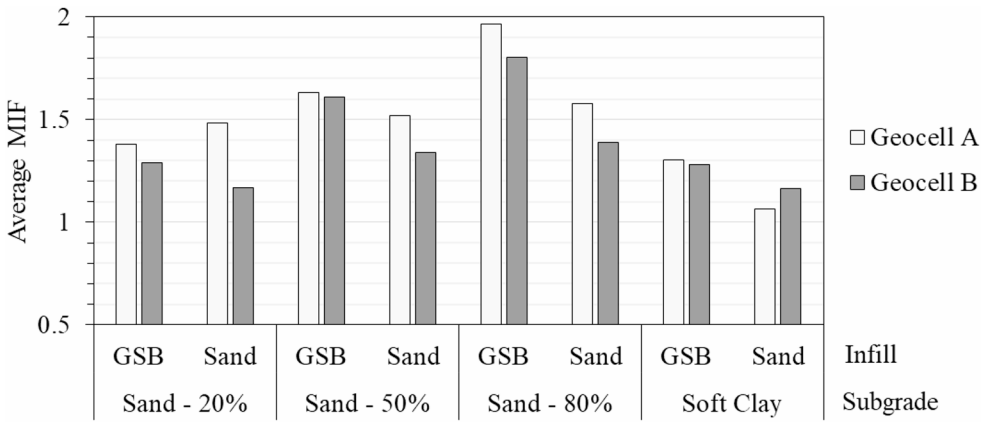

Fig. 4 Influence of geocell geometry on average MIF for GSB and sandy soil in different subgrade conditions

assess the interdependence of different relevant variables was performed using analytical tools that rely on machine learning algorithms, in line with recent studies highlighting the growing application of machine learning techniques in geotechnical engineering [49–51].

This evaluation employed the Multilayer Perceptron (MLP) model, a commonly adopted type of neural network, characterized by its effectiveness and robustness [52, 53]. The MLP models have been adopted in scientific data analysis involving classification, regression and pattern recognition in a variety of fields, including geosynthetics applications such as geocells [26, 27, 52, 54].

The present study used MLP models to interpret the results collected from the 128 PLTs in order to facilitate MIF predictions as a function of the relevant variables governing the performance of geocell-reinforced layers. A Python code was developed to implement the MPL models, leveraging the open-source library TensorFlow and its high-level Application Programming Interface (API) Keras. The code was based on the steps and recommendations for scalar regression [54]. Initially, covariates were normalized using the Max Absolute Scaling method, consistent with the common practice in Deep Neural Networks (DNN) of using normalization techniques on the data set to optimize training speed and to generalize the models [55]. The architecture of the models, built using the Keras functional API, consisted of an input layer with two features, corresponding to the variables E_{un} and E_s, followed by dense hidden layers employing Rectified Linear Unit (ReLU) activation functions. The ReLU functions were selected to mitigate difficulties related to vanishing gradients and capture non-linear relationships [54, 56]. Lastly, the output layer, responsible for returning MIF predictions, consisted of a single neuron without activation function. It is worth noting that the MLP models were trained using only E_{un} and E_s as input features, although including additional inputs could potentially enhance model generalization.

The models were compiled using the Adaptive Moment Estimation (Adam) optimizer and Mean Squared Error (MSE) loss function. Training was conducted for 1,000 epochs using the backpropagation algorithm, with a 25% data split for validation and testing. Although more advanced validation approaches, such as k-fold cross-validation, could provide a more robust assessment of generalization, the hold-out split adopted in this study is consistent with recent geotechnical applications of neural networks, including studies on geosynthetics such as geocells [26, 28]. Hyperparameters, including the number of hidden layers, number of neurons, regularization parameter, and random seeds, were tuned based on multiple metrics, such as MSE, and the coefficient of determination (R^2). The model selection process aimed at minimizing high variance (overfitting) and high bias (underfitting) while also ensuring adequate generalization.

Figure 5 presents the evolution of the MSE and R^2 during the model training for the cases involving Geocell A with sandy soil infill. For this specific case, the training MSE showed a significant reduction with increasing epochs until approximately epoch 200, beyond which, the reduction became marginal. However, at this point the validation MSE was comparatively high, indicating a high variance of the model. This variance was also evidenced in the R^2 of the training data, which had a low value initially until Epoch 200, but continued to increase until a peak value of 0.90 was reached. Both results show that training with approximately 1,000 epochs could be considered adequate to reach convergence, with a marginally higher validation MSE than training MSE (0.0153 and 0.0098, respectively, for Epoch 1000), indicating a robust fit. A similar procedure was applied to the other cases. The average MSE and R^2 obtained at the end

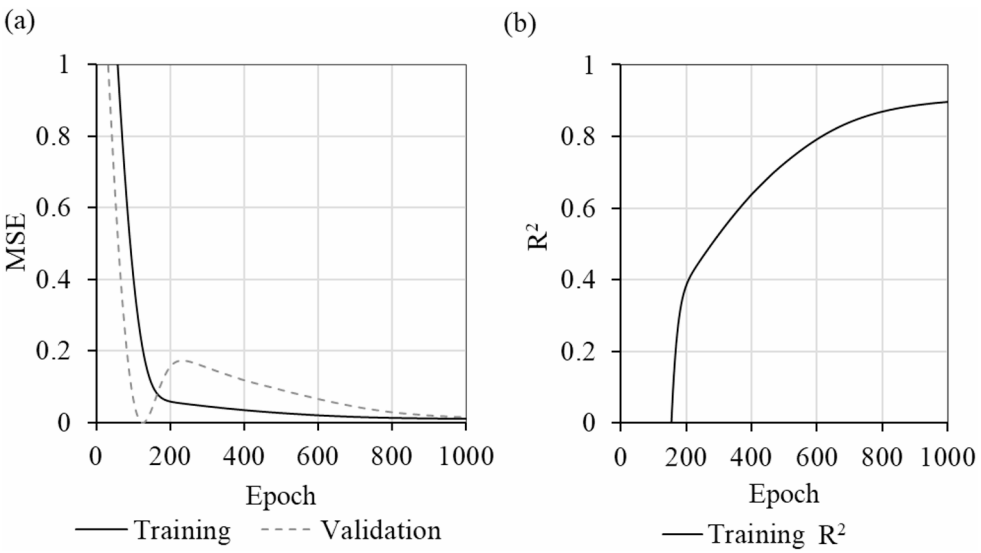

Fig. 5 Training metrics of the MLP model for sandy soil reinforced with Geocell A: **a** evolution of MSE for training and validation data sets; and **b** R^2 score evolution

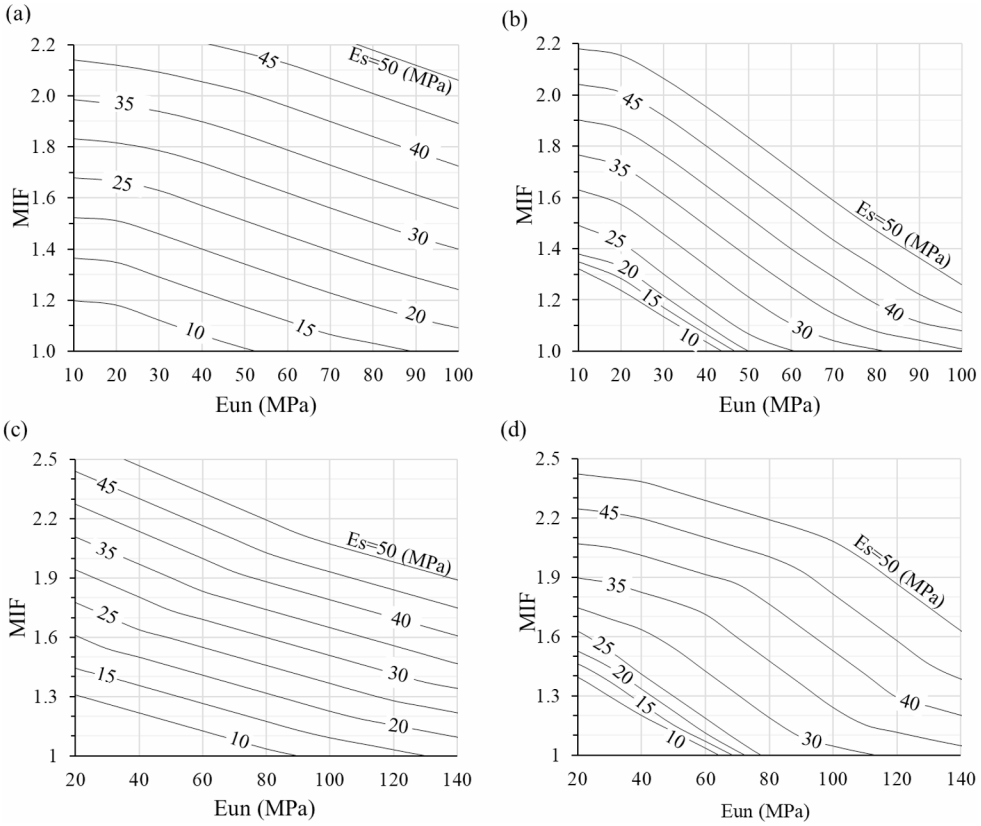

Fig. 6 Combined effect of influence factors on predictive MIF values after MLP deep learning: **a** Geocell A with sandy soil infill, **b** Geocell B with sandy soil infill, **c** Geocell A with GSB infill, **d** Geocell B with GSB infill

of the training of all models were 0.009 and 0.87, respectively. These models were further evaluated for the test set, with MSE values ranging from 0.00004 to 0.0346 (average of 0.01), suggesting a good generalization.

The trained models were utilized to make predictions and generate the charts presented in Fig. 6, which show contour plots depicting the relationship between the influence factors and predicted MIF values. The influence of the infill material and subgrade were captured by their modulus, E_{un} and E_s, respectively. Each contour line represents a constant value of E_s, as indicated by the labels (e.g., from 10 MPa to 50 MPa, in increments of 5 MPa). Figure 6a and b present the results corresponding to cases involving the use of sandy soil infill for Geocells A and B, respectively. Figure 6c and d show analogous results corresponding to cases involving the use of GSB infill. These charts were calculated from PLT results, which were obtained with a marginally compaction stress compared to that typically adopted in the field and works. It should be noted that the efficient compaction process is expected to significantly impact MIF values.

From the trends observed in Fig. 6, it can be noted that the MIF increases with increasing values of E_s, decreases with increasing values of d_{eq} (d_{eq} Geocell A < d_{eq} Geocell B) and decreases with increasing values of E_{un}. These trends were previously observed in the PLT experimental program, as discussed earlier, and are consistent with trends reported in other studies [9]. Figure 6 indicates that, for a given change in E_s or E_{un} value, the E_s has a greater influence than E_{un} on the predicted MIF values. However, due to the larger range of variation in E_{un}, the effect of E_{un} becomes significant. The absence of high compaction stress increases the sensitivity of MIF to subgrade stiffness, corroborating the observations from the experimental program. Moreover, Geocell B presented a different pattern than Geocell A for comparatively low E_s values for both infill materials. This difference is probably due to the reduced confinement provided by greater pocket size of Geocell B under loading. This behavior is due to the absent high compactive effort, which encapsulate confinement stresses inside the geocell pocket, and to the very low subgrade modulus associated with larger pocket sizes, that generates a lack of confinement at the base of the reinforced layer, reducing reinforcement efficiency.

Limitations

This study has certain limitations that must be considered when interpreting the results. The MIF evaluation was specifically designed to investigate the influence of parameters, including elastic moduli of subgrade and infill material, and geocell dimensions, under controlled laboratory conditions.

Importantly, the compaction level applied to the infill materials during test preparation was significantly lower than that typically used in field applications, which limit the representativeness of the obtained MIF values. Additional tests with field-equivalent compactive stresses are needed to validate the predictive charts for practical design use.

Additionally, the analysis was constrained by a limited number of influencing parameters and materials (e.g., one source of soft clay, one sand source, and one source of GSB). This restricted scope further limits the applicability of the results beyond the experimental conditions studied herein.

Therefore, the results may not fully represent the variability of conditions encountered in practical applications, especially in real works. The MIF values reported in this research should be regarded as tools for comparative and parametric analyses to explore the behavior of geocell-reinforced systems. They are not intended for direct application as design values in engineering projects. Further studies are recommended to explore a broader range of influencing parameters, including representative compaction levels and a wider variety of subgrade and infill material types, as well as different geocell configurations.

Conclusions

This study presented the results and evaluation of Plate Load Tests (PLTs) conducted with unreinforced and geocell-reinforced coarse materials, considering several infill materials, subgrades, and geocell types. Specifically, static PLTs were conducted on laboratory model with two load-unload cycles following the German standard DIN 18134. Subgrade conditions included a soft clay and sandy soil at three different relative densities. The upper layer consisted of a sandy soil and GSB at two different densities each. Two geocells manufactured using HDPE with different heights and pocket sizes were adopted. A total of 128 tests were conducted aiming at investigating the influence of the subgrade, infill material and geocell dimensions on the MIF. A back-calculation procedure based on an extension of the Boussinesq equation and the two-layered elastic system theory was used to determine the moduli of the different subgrades and top layers in both reinforced and unreinforced conditions. An analysis of the combined effects of subgrade, infill and geocell dimensions was conducted using Multilayer Perceptron (MLP), a deep learning technique, with the resultant MIF predictions presented in the form of charts. Based on the results and discussion, the following conclusions can be made:

- Even though the compaction stress during infill placement was marginally, probably not resulting on modulus improvement typical of field compaction operations, MIF values as high as 2.1 were obtained.
- The subgrade type and conditions were found to significantly influence the magnitude of the unreinforced modulus, also probably due to the use of comparatively low compactive efforts on the top layer, which was also reflected in the MIF values.
- As expected, the experimental results confirmed the significant influence of the infill material on the MIF. Although the unreinforced and reinforced moduli for both infill materials were lower than those under typical field compaction operations, MIF values increased with decreasing infill density. This indicates that unbound granular materials with comparatively low modulus, such as sand infill or those commonly used in subbase layers, may experience comparatively greater improvement (higher MIF) when using geocells than unbound granular materials typically used in base layers.
- Geocell A, with a comparatively smaller equivalent diameter (d_{eq}), consistently exhibited a higher MIF compared to Geocell B, with MIF values up to 27% higher (8% higher on average).
- The Multilayer Perceptron (MLP) models were found to effectively predict the MIF as a function of parameters E_s and E_{un} for Geocells A and B. Charts could be generated by the deep learning models, confirming the trends observed in the experimental program. Overall, the use of data science concepts such as the MLP, on geosynthetic applications proved to be a valuable tool to conduct parametric analyses.

Acknowledgements The authors would like to acknowledge the Wavin Geosynthetics for supporting the experimental program, and the support provided by the São Paulo Research Foundation (FAPESP grant 2023/04447-1), the National Council of Scientific and Technological Development (CNPq grant 305309/2024-2), and the Coordination for the Improvement of Higher Education Personnel - Brazil.

Author Contributions H. D. Trujillo contributed to the investigation, original draft preparation, and manuscript review and editing. J. O. Avesani Neto contributed to the conceptualization, supervision, and manuscript review and editing. J. G. Zornberg contributed to validation and manuscript review and editing.

Data Availability Data will be made available upon reasonable request.

Declarations

Competing Interests The authors declare that they have no known competing financial interests or personal relationships that could have appeared to influence the work reported in this paper.

References

1. Babagiray G, Oguzhan Akbas S, Anil O (2023) Full-scale field impact load experiments on buried pipes in geosynthetic-reinforced soils. Transp Geotech 38:100927. https://doi.org/10.1016/j.trgeo.2022.100927
2. Khan MA, Puppala AJ (2023) Sustainable pavement with geocell reinforced reclaimed-asphalt-pavement (RAP) base layer. J Clean Prod 387:135802. https://doi.org/10.1016/j.jclepro.2022.135802
3. Krishna A, Latha GM (2023) Evolution of geocells as sustainable support to transportation infrastructure. Sustainability 15:11773. https://doi.org/10.3390/su151511773
4. Menon V, Kolathayar S (2024) Optimizing nailing parameters for hybrid retaining systems using supervised learning regression models. Multiscale Multidiscip Model Exp Des. https://doi.org/10.1007/s41939-024-00417-3
5. Saikia R, Dash SK (2024) Load carrying mechanism of geocell reinforced embankment on soft soil. Transp Res Rec J Transp Res Board 2678:462–480. https://doi.org/10.1177/03611981241230317
6. Song G, Song X, He S et al (2022) Soil reinforcement with geocells and vegetation for ecological mitigation of shallow slope failure. Sustainability 14:11911. https://doi.org/10.3390/su141911911
7. Baby LM, Avesani Neto JO (2024) Evaluation of geocell-reinforced railway track using FEM and FLM-based software: a parametric analysis. Int J Geosynth Ground Eng 10:1–9. https://doi.org/10.1007/s40891-024-00564-0
8. Rezende JCV, Avesani Neto JO, Zornberg JG (2024) Shear strength characterization of the interface between geocell walls and infill. Indian Geotech J. https://doi.org/10.1007/s40098-024-01108-z
9. Vega E, van Gurp C, Kwast E (2018) Geokunststoffen Als funderingswapening in Ongebonden funderingslagen (Geosynthetics for reinforcement of unbound base and subbase pavement Layers). SBRCUR/CROW
10. Zornberg JG (2017) Functions and applications of geosynthetics. Roadways Procedia Eng 189:298–306. https://doi.org/10.1016/j.proeng.2017.05.048
11. AASHTO (2015) Mechanistic-Empirical Pavement Design Guide -Second edition. Am. Assoc. State Highw. Transp. Off., Washington, DC, p 227
12. Austroads (2024) Guide to Pavement Technology Part 2: Pavement Structural Design. Australia
13. Mahima D, Sini T (2022) Performance evaluation of demolition waste infilled geocell-reinforced subgrade by flexural and rutting analysis. Road Mater Pavement Des 23:1746–1761. https://doi.org/10.1080/14680629.2021.1924233
14. Saride S, Baadiga R, Balunaini U, Madhira MR (2022) Modulus improvement factor-based design coefficients for geogrid- and geocell-reinforced bases. J Transp Eng Part B Pavements 148:1–14. https://doi.org/10.1061/JPEODX.0000380
15. Gottumukkala B, Mehar B, Minchala D et al (2023) Laboratory and field evaluations of geocell reinforced bases for locally available material in the Himalayan Region. Int J Geosynth Ground Eng 9:74. https://doi.org/10.1007/s40891-023-00497-0
16. Pokharel SK, Han J, Leshchinsky D, Parsons RL (2018) Experimental evaluation of geocell-reinforced bases under repeated loading. Int J Pavement Res Technol 11:114–127. https://doi.org/10.1016/j.ijprt.2017.03.007
17. Zipoli LLR, Avesani Neto JO (2022) Evaluation of back-calculated elastic moduli of unreinforced and geocell-reinforced unbound granular material from full-scale field tests. Geotext Geomembr 50:910–921. https://doi.org/10.1016/j.geotexmem.2022.05.006
18. Feng LX, Avesani Neto JO, Zornberg JG (2024) Evaluation of the elastic modulus improvement in geocell-reinforced unbound aggregates: full-scale experimental sections on a highway. Transp Geotech 49:101444. https://doi.org/10.1016/j.trgeo.2024.101444
19. Garcia RS, Avesani Neto JO (2021) Stress-dependent method for calculating the modulus improvement factor in geocell-reinforced soil layers. Geotext Geomembr 49:146–158. https://doi.org/10.1016/j.geotexmem.2020.09.009
20. Schary Y (2020) Guidelines for the Use and Design of Geocells in Road Reinforcement Applications. In: Sitharam, T., Hegde, A., Kolathayar, S. (eds) Geocells. Springer Transactions in Civil and Environmental Engineering. 367–386. https://doi.org/10.1007/978-981-15-6095-8_14
21. IRC:SP:59 (2019) Guidelines for use of geosynthetics in road pavements and associated works (First Revision). Indian Roads Congress. https://law.resource.org/pub/in/bis/irc/irc.gov.in.sp.059.2018.pdf
22. Biswas S, Hussain M, Singh KL (2023) Performance evaluation of infill materials of Geocell-reinforced granular bed overlying soft subgrade. Indian Geotech J 53:651–664. https://doi.org/10.1007/s40098-022-00695-z
23. Evirgen B, Kara HO, Ucun MS et al (2024) The effect of the geometrical properties of geocell reinforcements between a two-layered road structure under overload conditions. Case Stud Constr Mater. https://doi.org/10.1016/j.cscm.2023.e02793
24. Fazeli Dehkordi P, Ghazavi M, Karim UFA (2022) Bearing capacity-relative density behavior of circular footings resting on geocell-reinforced sand. Eur J Environ Civ Eng 26:5088–5112. https://doi.org/10.1080/19648189.2021.1884901
25. Jeyanthi S, Venkatakrishnaiah R, Raju KVB (2023) Utilising recurrent neural network technique for predicting strand settlement on brittle sand and geocell. Int J Intell Eng Inf 11:122–137. https://doi.org/10.1504/IJIEI.2023.132699
26. Sheikh IR, Wani KMNS, Jalal FE, Shah MY (2022) An investigation on the behaviour of geosynthetic reinforced quarry waste bases (QWB) under vertical loading. Environ Sci Pollut Res 29:43385–43400. https://doi.org/10.1007/s11356-021-18238-z
27. Sheikh IR, Shah MY (2023) Experimental and artificial neural network analysis of geocell reinforcement on deformation and vertical stress distribution of quarry waste base. Soil Mech Found Eng 60:362–368. https://doi.org/10.1007/s11204-023-09902-2
28. Ghani S, Kumari S, Choudhary AK (2024) Geocell mattress reinforcement for bottom ash: a comprehensive study of Load-Settlement characteristics. Iran J Sci Technol Trans Civ Eng 48:727–743. https://doi.org/10.1007/s40996-023-01205-8
29. DIN 18134 (2012) Soil - Testing procedures and testing equipment- Plate load test, English translation of DIN 18134:2012-O4. Dtsch. Inst. für Normung 25
30. Trujillo HD (2025) Evaluation of influence parameters on the modulus improvement factor of geocell-reinforced granular soils based on laboratory plate load tests and supervised machine learning. https://doi.org/10.11606/D.3.2025.tde-03092025-073923. Master's dissertation. Universidade de São Paulo
31. Kulhawy FH, Mayne PW (1990) Manual on Estimating Soil Properties for Foundation Design. Report Number: EPRI-EL-6800. https://www.osti.gov/biblio/6653074
32. Bowles Joseph E. (1997) Foundation Analysis and Design, Fifth Edition. McGraw-Hill, Peoria, Illinois
33. Yamamuro JA, Lade PV (1997) Static liquefaction of very loose sands. Can Geotech J 34:905–917. https://doi.org/10.1139/t97-057
34. Avesani Neto JO (2019) Application of the two-layer system theory to calculate the settlements and vertical stress propagation in soil reinforcement with geocell. Geotext Geomembr 47:32–41. https://doi.org/10.1016/j.geotexmem.2018.09.003

35. Huang YH (2004) Pavement Analysis and Design, Second edi. Pearson Education, Inc
36. Saride S, Gautam D, Madhav MR, Vijay KR (2016) Performance evaluation of geocell reinforced granular subbase (GSB) layers through field trials. J Indian Roads Congr 76(4):249–257
37. Yoder EJ, Witczak MW (1975) Principles of Pavement Design. John Wiley & Sons, Inc., Hoboken, NJ, USA
38. ASTM (2021) D8269-21: Standard Guide For The Use Of Geocells In Geotechnical And Roadway Projects. i:1–11. https://doi.org/10.1520/D8269-21.2
39. USACE (1990) Settlement analysis. EM 1110-1-1904. https://www.publications.usace.army.mil/Portals/76/Publications/EngineerManuals/EM_1110-1-1904.pdf
40. Lee IK, White W, Ingles OG (1983) Geotechnical Engineering. Pitman Publishing Inc, Massachusetts
41. Duncan JM, Byrne P, Wong KS, Mabry P (1980) Strength, stress-strain and bulk modulus parameters for finite analyses of stresses and movements in soil masses. Report No. UCB/GT/BO-O. College of Engineering, University of California, Berkeley, CA
42. Duncan JM, Chang C-Y (1970) Nonlinear analysis of stress and strain in soils. J Soil Mech Found Div 96:1629–1653. https://doi.org/10.1061/jsfeaq.0001458
43. Janbu N (1963) Soil compressibility as determined by oedometer and triaxial tests. In: Proceeding of the European Conference on Soil Mechanics and Founation Engineering (ECSMFE). pp 19–25
44. Giroud JP, Han J (2004) Design method for geogrid-reinforced unpaved roads. I. Development of design method. J Geotech Geoenviron Eng 130:775–786. https://doi.org/10.1061/(ASCE)1090-0241(2004)130:8(775)
45. STAC (2016) Rational design methodology for flexible airfield pavement. Technical guide. The French Civil Aviation Technical Center
46. IRA (2003) Design guidelines for asphalt highway structural pavements. Israel Road Authority, Tel Aviv
47. Shell (1978) Shell Pavement Design Manual: Asphalt Pavements and Overlays for Road Traffic. Shell International Petroleum Company Limited, London, England
48. Zhao Y, Lu Z, Liu J et al (2024) Compaction-induced prestressing effect of geocell reinforcement. Geosynth Int 1–48. https://doi.org/10.1680/jgein.24.00082
49. Raja MNA, Mercado V, Abdoun T, El-Sekelly W (2025) Seismic site amplification prediction- an integrated bayesian optimisation explainable machine learning approach. Georisk Assess Manag Risk Eng Syst Geohazards 19:573–592. https://doi.org/10.1080/17499518.2025.2521870
50. Raja MNA, Abdoun T, El-Sekelly W (2024) Smart prediction of liquefaction-induced lateral spreading. J Rock Mech Geotech Eng 16:2310–2325. https://doi.org/10.1016/j.jrmge.2023.05.017
51. Banerjee L, Chawla S, Dash SK (2023) Investigations on cyclic loading behavior of geocell stabilized tracks with coal overburden refuse recycled as subballast material. Transp Geotech 40:100969. https://doi.org/10.1016/j.trgeo.2023.100969
52. Du K-L, Leung C-S, Mow WH, Swamy MNS (2022) Perceptron: learning, Generalization, model Selection, fault Tolerance, and role in the deep learning era. Mathematics 10:4730. https://doi.org/10.3390/math10244730
53. Turner R (2019) Python machine learning: the ultimate beginner's guide to learn python machine learning. Step by Step using Scikit-Learn and Tensorflow
54. Chollet F (2021) Deep Learning with Python. Manning Publications Co
55. Huang L, Qin J, Zhou Y et al (2023) Normalization techniques in training DNNs: methodology, analysis and application. IEEE Trans Pattern Anal Mach Intell 45:10173–10196. https://doi.org/10.1109/TPAMI.2023.3250241
56. Goulet J-A (2020) Probabilistic Machine Learning for Civil Engineers. The MIT Press, Cambridge
57. PAVCO (2021) Refuerzo en carreteras Geoceldas. In: Geocelda_FT2021. https://pavcowavingeosinteticos.com/wp-content/uploads/2021/12/Geocelda_FT2021.pdf